SCIENCE CHINA Materials

LETTER

mater.scichina.com link.springer.com

Published online 16 August 2017 | doi: 10.1007/s40843-017-9082-1
Sci China Mater 2017, 60(9): 903–908

Atomic layer reversal on CeO_2 (100) surface

Jinglu Huang[1], Yunbo Yu[2,3,4], Jing Zhu[1] and Rong Yu[1*]

ABSTRACT **The structure and properties of CeO_2 surfaces have been intensively studied due to their importance in a lot of surface-related applications. Since most of surface techniques probe the structure information inside the outermost surface plane, the subsurface structure information has been elusive in many studies. Using the profile imaging with aberration-corrected transmission electron microscopy, the structure information in both the outermost layer and the sublayers of the CeO_2 (100) surface has been obtained. In addition to the normal structures that have been reported before, where the surface is Ce- or O-terminated, a metastable surface has been discovered. In the new structure, there is an atomic layer reversal between the outermost layer and the sublayer, giving a structure with O as the outermost layer for the stoichiometry of normal Ce-terminated surface. The charge redistribution for the polarity compensation has also been changed relative to the normal surface.**

Keywords: surface structure, ceria, atomic layer reversal, aberration-corrected TEM, first-principles calculations

Materials based on CeO_2, owing to their outstanding physical and chemical properties, have played important roles in solar cells [1], solid-oxide fuel cells [2,3], UV blockers [4–6] and a variety of catalytic reactions like three-way automotive catalytic converters, the production and purification of hydrogen [7–10]. Many of these applications are closely related to the specific local structures on CeO_2 surface such as islands, steps, oxygen vacancies and Ce^{3+} ions. For instance, the high capacity of CeO_2 in oxygen storage-release is largely contributed by the oxygen vacancies that can be quickly formed and eliminated [11]; the abundant oxygen vacancies in Ru/CeO_2 catalysts serve as the active site for CO_2 activation [12] and also behave as the active sites for many catalytic reactions with the accompanied reduction of Ce^{4+} ions [13]; the high activity of Au/ceria catalysts in the water-gas shift reaction has been traced back to the ionic Au species that only strongly associated with cerium-oxygen surface [14,15]. Hence, CeO_2 surfaces have been attracting large amount of investigation. In previous studies on the surface of CeO_2, single crystals were usually chosen as the main research objects. Scanning tunneling microscope (STM) and atomic force microscope (AFM) were commonly used in structural characterization [16–18]. Most of research findings are focused on the (111) surface of ceria single crystals or epitaxial thin films. Namai *et al.* [16,17] observed the structure and dynamic behavior of CeO_2 (111) surfaces in STM, and visualized the surface oxygen atoms, oxygen point defects, and multiple oxygen defects on oxygen-terminated CeO_2 (111) surface through noncontact AFM. Esch *et al.* [18] unraveled the local structure of oxygen vacancies on the (111) surface and subsurface combining high resolution STM with density functional calculations. They found that the electrons left behind by released oxygen localized on and reduced cerium ions, primarily by inducing subsurface vacancies, which played a crucial role in the formation of vacancy clusters on ceria substrates.

In real applications, most catalytic materials are used in the form of micro- or nano-crystals. Due to the size effect, there would be many differences between the surface structure of single crystals and those of micro- or nano-crystals. A recent example is the formation of the hcp structure in Rh nanoparticles, although the bulk Rh has the fcc structure [19]. In order to have a deeper understanding about the local structures and properties of ceria in engineering applications, we need to pay more attention to ceria with different sizes and morphologies. High resolution transmission electron microscopy (HRTEM) has been

[1] National Center for Electron Microscopy in Beijing, Key Laboratory of Advanced Materials of Ministry of Education of China and State Key Laboratory of New Ceramics and Fine Processing, School of Materials Science and Engineering, Tsinghua University, Beijing 100084, China
[2] State Key Joint Laboratory of Environment Simulation and Pollution Control, Research Center for Eco-Environmental Sciences, Chinese Academy of Sciences, Beijing 100085, China
[3] Center for Excellence in Regional Atmospheric Environment, Institute of Urban Environment, Chinese Academy of Sciences, Xiamen 361021, China
[4] University of Chinese Academy of Sciences, Beijing 100049, China
* Corresponding author (email: ryu@tsinghua.edu.cn)

used to study the atomic structures of the surfaces of CeO_2 nanoparticles, and has revealed structural details with increasing spatial resolution. Recently, aberration-corrected transmission electron microscopy (TEM) has been able to distinguish the Ce columns at the surface of CeO_2 nanoparticles. Lin *et al.* [20] successfully observed the Ce and O atom columns on {100}, {110} and {111} ceria surfaces with aberration-corrected TEM. The {100} surfaces were shown to have a complex structure, with mixed Ce-, O-, and CeO-terminations. The {110} surfaces have large amount of oxygen vacancies and easily form {111} nanofacets to lower the surface energy. The {111} surfaces were always terminated by O atoms. Haigh *et al.* [21] also characterized several low index surfaces of CeO_2 in AFM and aberration-corrected TEM. They found that the O-terminated {111} surfaces could keep stable, while the Ce-terminated {100} surfaces were unstable.

In this study, the (100) surfaces of CeO_2 have been investigated combining aberration corrected TEM and first-principles calculations. Various surface structures have been identified. In addition to the normal (100) surface that has Ce or O as the outermost layer, a new surface structure with the atomic layer reversal has been revealed.

The CeO_2 nanoparticles were prepared though a hydrothermal process, using $Ce(NO_3)_3{\cdot}6H_2O$ and NaOH solution with a concentration of 1 mol L^{-1} as the reactants. The specific synthesis steps were introduced in the reference [22]. HRTEM images were taken on an FEI Titan 80-300 microscope equipped with a CEOS image aberration-corrector. The operating voltage was 300 kV and the spherical aberration was set to −13 μm. The image simulation of relaxed surface models was performed using the MacTempasX software.

Calculations of the bulk and surface relaxations of CeO_2 were carried out using the projector augmented-wave (PAW) method [23] within the density functional theory (DFT), as implemented in the VASP code [24,25]. In order to consider the strongly correlated 4f electrons of Ce in CeO_2, calculations were performed using the GGA+U approximation, with the on-site Coulombic interaction parameter U set to be 5 eV. As noted by Andersson *et al.* [26] and Zhang *et al.* [27], although suggestions of U values vary in literature, the optimal ones appear to be around 5.0 eV for GGA+U. For the (100) surface, supercells of 3.873 Å × 3.873 Å × 47.387 Å was used. The supercells have a crystal slab of about 27 Å thick, and a vacuum layer of 20 Å thick.

Fig. 1a shows an experimental aberration-corrected TEM image of the (100) surface of a CeO_2 nanoparticle. Fig. 1b shows the simulated images of CeO_2 in the same direction, with the focus in the range of 0 and 10.0 nm, and the thickness in the range of 0.3 and 2.7 nm. The comparison between the experimental and simulated images indicates that the focus and thickness for the experimental image is about 7.0 and 1.9 nm, respectively. At this condition, there is a one-to-one correspondence between the intensity maxima in the image and the projected atomic positions in the viewing direction. The strong and weak spots are Ce and O atom columns, respectively. They are well resolved, enabling us to perform accurate measurements and structural analysis.

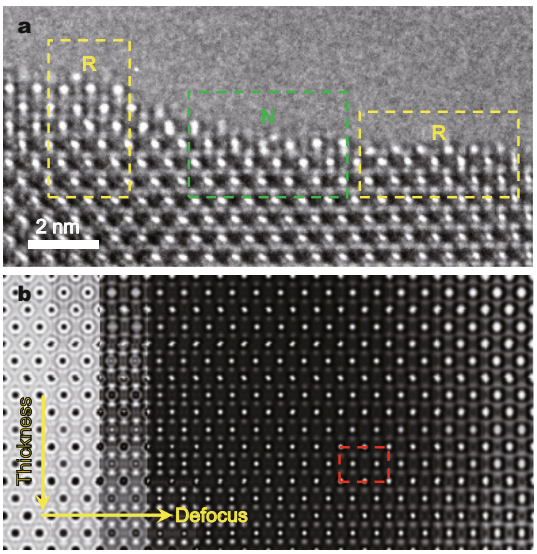

Figure 1 (a) Experimental aberration-corrected TEM image of the CeO_2 (100) surface, viewed in the [011] zone axis. (b) Simulated images of CeO_2 in the [011] zone axis. Two types of surface structure can be identified in the experimental image, as labelled N (normal) and R (reversed), respectively.

Two types of surface structures can be identified in Fig. 1a, as labelled N and R, respectively. Fig. 2a shows the enlarged N area. As can be seen, the atomic configuration extends from the bulk up to the outermost layer, indicating that a cleaved surface is formed. The spacing between the first and the second Ce atomic layers was measured to be 2.69 Å, which is very close to the corresponding to the bulk value (2.71 Å).

The (100) surface of CeO_2 is a type 3 polar surface according to Tasker's classification [28]. The polarity needs to be compensated to lower the surface energy. To compensate the polarity of the Ce-terminated surface, negative charges $2e^-$ per surface unit cell are required, which can be realized by reducing two Ce^{4+} ions to Ce^{3+}. For the O-terminated surface, an O vacancy per surface unit cell is required. The ordering of the vacancies would lead to the $(\sqrt{2} \times \sqrt{2})$ R45° reconstructed CeO structure.

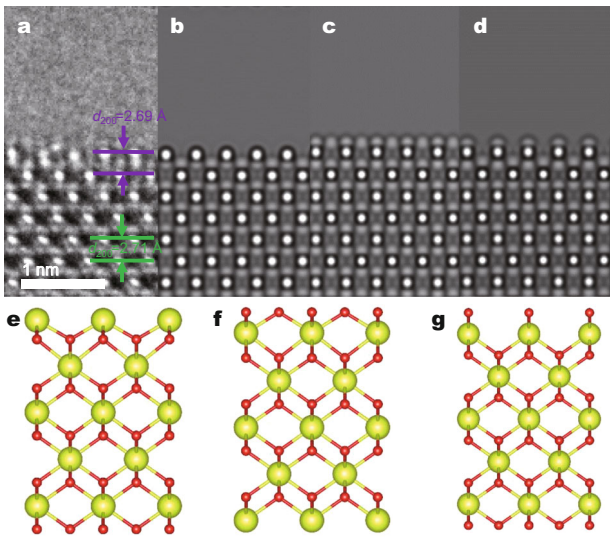

Figure 2 (a) The enlarged image of the cleaved (100) surface of CeO_2, with a slight inward relaxation of the surface layers; (b–d) The simulated images of the Ce-terminated, full O-terminated, and half O-terminated [$(\sqrt{2}\times\sqrt{2})$ R45°] surfaces, which are relaxed with first-principles calculations. The corresponding models are shown in (e–g).

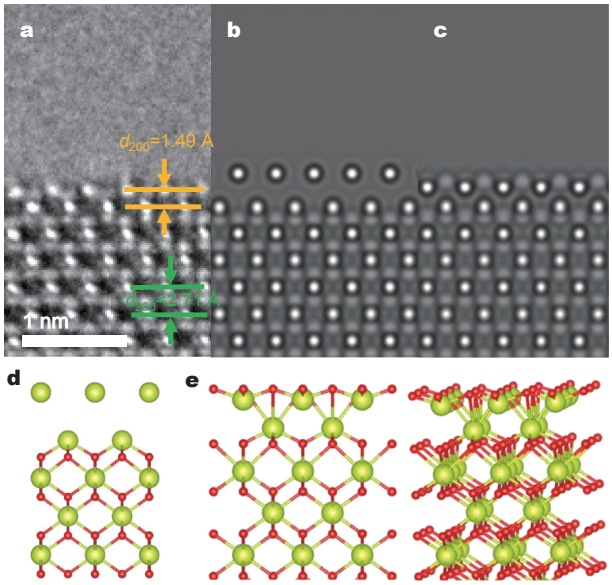

Figure 3 (a) The enlarged image of the reversed (100) surface of CeO_2, with a huge inward relaxation of the outermost Ce layer. (b) and (c) The simulated image of the model relaxed with first-principles calculations shown in (d) and (e), respectively.

Considering the experimental observations and above discussion, three types of surface models were constructed, with Ce-termination, full O-termination, and half O-termination, respectively. Prior to the relaxation of the surface models, the lattice parameter of bulk CeO_2 was optimized first. The results give a = 0.548 nm, slightly (1.3%) larger than the experimental value (0.541 nm), consistent with usual error given by the PBE functional. Fig. 2e–g show the relaxed models for the three surface models, respectively. For the Ce-terminated surface, the topmost Ce relaxes inward by 8 pm, and the O sublayer relaxes outward by 16 pm, shortening the spacing between the first two atomic layers from 1.37 to 1.12 Å. For the full O-terminated surface, the topmost O relaxes inward by 4 pm, and the Ce sublayer relaxes outward by 12 pm, shortening the spacing between the first two atomic layers from 1.37 to 1.21 Å. Larger relaxations occur for the half O-terminated $(\sqrt{2}\times\sqrt{2})$ R45° surface, and the spacing between the first two atomic layers was shortened from 1.37 to 1.04 Å.

For both full and half O-terminated structures, the surface atoms have slight changes in the charge state. For the Ce-terminated surface, however, the first two Ce atoms were reduced from Ce^{4+} to Ce^{3+}, consistent with the prediction for the polarity compensation. Due to the localized 4f electron on the Ce^{3+} ions, the convergence in the calculations of the Ce-termination is much lower than the other two surfaces.

There is a weak contrast above the topmost Ce atomic layer, indicating that the surface can be viewed as Ce-terminated one with O adatoms, or O-terminated one with O vacancies. In order to discriminate the three models, accurate measurements of the image intensity and the positions of the atomic columns are required. The signal to noise ratio of Fig. 2a is not high enough for this purpose. As noted before [20,29–32], however, the mobility of atoms at ceria (100) surface is quite high and the three types terminations discussed above could coexist at the surface. In fact, the mobility of oxygen inside CeO_2 is also high, making it a good oxygen reservoir in catalytic applications or ionic conductor in solid oxide fuel cells [33]. The contribution of entropy to the structural stability and polarity compensation is also important for such surfaces with a lot of adatoms or vacancies [34,35].

Fig. 3a shows the enlarged R area. In contrast to the cleaved surface that has slight relaxation, there is a surprisingly huge relaxation of the topmost Ce layer in the R areas. The spacing between the first two Ce layers was measured to be 1.49 Å, much less than the bulk value (2.71 Å).

Based on the experimental measurements, several models have been built considering the stacking sequence of O and Ce layers and the amount of oxygen vacancies. The models were then optimized with the first-principles calculations. Two of the relaxed structures are shown in

Fig. 3d, e. Most of the structures are not able to reproduce the huge relaxation of the outermost Ce layer. Fig. 3d is an example, where the spacing between the first two Ce layers is 3.42 Å, much larger than the experimental value (1.49 Å).

The only structure that can reproduce the huge relaxation is the model shown in Fig. 3e. The corresponding simulated image is given in Fig. 3c, which matches reasonably well the experimental image. The spacing between the first two Ce atomic layers was 1.87 Å, close to the experimental value (1.49 Å). The structure has the same surface stoichiometry as the Ce-terminated surface, but the original O sublayer moves cross the Ce layer to form the new outermost O layer.

As a metastable structure, the reversed surface has an energy higher than the normal Ce-terminated surface by 1.5 J m^{-2}. The charge redistribution for the polarity compensation is also different. For the normal Ce-terminated surface, the reduction of the surface Ce^{4+} ions involves primarily the occupancy of the 4f orbitals of the surface Ce ions. Due to the change of the coordination of the outermost Ce ion in the reversed surface, however, the reduced Ce ions have more occupancy in the 5d orbitals, and have no local magnetic moment. The Ce ions in the sublayers have more occupancy in the 4f orbitals, and have a local magnetic moment of 0.9 Bohr magneton.

The formation of the reversed surface can be rationalized considering the bonding between the neighbors, and the valence change of the subsurface Ce atoms. For the normal surface, each Ce atom has 8 O neighbors and each O atom has 4 Ce neighbors. This neighboring relation remains in the reversed surface. The main difference lies in the elongated Ce–O bonds in the reversed surface compared with the normal surface, leading to the higher energy of the reversed surface. The Ce-Ce distance in the reversed surface is also shorter (although not as apparent as the projection shown in Fig. 3) than those in the normal structure, which would also contribute to the higher energy of the reversed structure. The valence change described above is an indication of the existence of covalence and weak ionicity. For the oxides with weak ionicity, the energy penalties for shorter bonds between like atoms are smaller than those in the oxides of strong ionicity. As a result, density-functional theory calculations show that the reversed structure is metastable. The force on all the atoms in the relaxed structure is zero, and the simulated image of the relaxed structure matches well with the experimental image.

In conclusion, two types of {100} surfaces of CeO_2 have been investigated combining aberration-corrected TEM and first-principles calculations. For the normal Ce- and O-terminated surfaces, the atomic relaxation is less than 0.2 Å. A huge surface relaxation has been revealed, with the spacing between the outermost Ce layer and the Ce sublayer reduced 50% relative to the bulk value. The structure has the same surface stoichiometry as the normal Ce-terminated surface, but the original O sublayer moved cross the original Ce outermost layer, forming a reversed structure with O as the termination.

Received 4 June 2017; accepted 24 July 2017; published online 16 August 2017

1 Corma A, Atienzar P, García H, *et al.* Hierarchically mesostructured doped CeO_2 with potential for solar-cell use. Nat Mater, 2004, 3: 394–397
2 Gorte RJ, Park S, Vohs JM. Direct oxidation of hydrocarbons in a solid-oxide fuel cell. Nature, 2000, 404: 265–267
3 Atkinson A, Barnett S, Gorte RJ, *et al.* Advanced anodes for high-temperature fuel cells. Nat Mater, 2004, 3: 17–27
4 Mohanty BC, Lee JW, Yeon DH, *et al.* Dopant induced variations in microstructure and optical properties of CeO_2 nanoparticles. Mater Res Bull, 2011, 46: 875–883
5 Zholobak NM, Shcherbakov AB, Bogorad-Kobelska AS, *et al.* Panthenol-stabilized cerium dioxide nanoparticles for cosmeceutic formulations against ROS-induced and UV-induced damage. J PhotoChem PhotoBiol B-Biol, 2014, 130: 102–108
6 Liu KQ, Kuang CX, Zhong MQ, *et al.* Synthesis, characterization and UV-shielding property of polystyrene-embedded CeO_2 nanoparticles. Optical Mater, 2013, 35: 2710–2715
7 Trovarelli A. Catalytic properties of ceria and CeO_2-containing materials. Catal Rev, 1996, 38: 439–520
8 Ratnasamy C, Wagner JP. Water gas shift catalysis. Catal Rev, 2009, 51: 325–440
9 Beckers J, Rothenberg G. Sustainable selective oxidations using ceria-based materials. Green Chem, 2010, 12: 939–948
10 Vivier L, Duprez D. Ceria-based solid catalysts for organic chemistry. ChemSusChem, 2010, 3: 654–678
11 Campbell CT, Peden CHF. Oxygen vacancies and catalysis on ceria surfaces. Science, 2005, 309: 713–714
12 Wang F, He S, Chen H, *et al.* Active site dependent reaction mechanism over Ru/CeO_2 catalyst toward CO_2 methanation. J Am Chem Soc, 2016, 138: 6298–6305
13 Cordeiro MAL, Weng W, Stroppa DG, *et al.* High resolution electron microscopy study of nanocubes and polyhedral nanocrystals of cerium(IV) oxide. Chem Mater, 2013, 25: 2028–2034
14 Si R, Flytzani-Stephanopoulos M. Shape and crystal-plane effects of nanoscale ceria on the activity of Au-CeO_2 catalysts for the water-gas shift reaction. Angew Chem Int Ed, 2008, 47: 2884–2887
15 Fu Q, Saltsburg H, Flytzani-Stephanopoulos M. Active nonmetallic Au and Pt species on ceria-based water-gas shift catalysts. Science, 2003, 301: 935–938
16 Namai Y, Fukui KI, Iwasawa Y. Atom-resolved noncontact atomic force microscopic and scanning tunneling microscopic observations of the structure and dynamic behavior of CeO_2(111) surfaces. Catal Today, 2003, 85: 79–91
17 Namai Y, Fukui K, Iwasawa Y. Atom-resolved noncontact atomic

force microscopic observations of CeO_2 (111) surfaces with different oxidation states: surface structure and behavior of surface oxygen atoms. J Phys Chem B, 2003, 107: 11666–11673
18 Esch F, Fabris S, Zhou L, *et al.* Electron localization determines defect formation on ceria substrates. Science, 2005, 309: 752–755
19 Huang JL, Li Z, Duan HH, *et al.* Formation of hexagonal-close packed (HCP) rhodium as a size effect. J Am Chem Soc, 2017, 139: 575–578
20 Lin Y, Wu Z, Wen J, *et al.* Imaging the atomic surface structures of CeO_2 nanoparticles. Nano Lett, 2014, 14: 191–196
21 Haigh SJ, Young NP, Sawada H, *et al.* Imaging the active surfaces of cerium dioxide nanoparticles. ChemPhysChem, 2011, 12: 2397–2399
22 Wang L, Wang Y, Zhang Y, *et al.* Shape dependence of nanoceria on complete catalytic oxidation of *o*-xylene. Catal Sci Technol, 2016, 6: 4840–4848
23 Blöchl PE. Projector augmented-wave method. Phys Rev B, 1994, 50: 17953–17979
24 Kresse G, Furthmüller J. Efficient iterative schemes for *ab initio* total-energy calculations using a plane-wave basis set. Phys Rev B, 1996, 54: 11169–11186
25 Kresse G, Furthmüller J. Efficiency of *ab-initio* total energy calculations for metals and semiconductors using a plane-wave basis set. Comp Mater Sci, 1996, 6: 15–50
26 Andersson DA, Simak SI, Johansson B, *et al.* Modeling of CeO_2, Ce_2O_3, and CeO_{2-x} in the LDA + U formalism. Phys Rev B, 2007, 75: 035109
27 Zhang C, Michaelides A, King DA, *et al.* Oxygen vacancy clusters on ceria: decisive role of cerium f electrons. Phys Rev B, 2009, 79: 075433
28 Tasker PW. The stability of ionic crystal surfaces. J Phys C-Solid State Phys, 1979, 12: 4977–4984
29 Skorodumova NV, Baudin M, Hermansson K. Surface properties of CeO_2 from first principles. Phys Rev B, 2004, 69: 075401
30 Nolan M, Grigoleit S, Sayle DC, *et al.* Density functional theory studies of the structure and electronic structure of pure and defective low index surfaces of ceria. Surf Sci, 2005, 576: 217–229
31 Bhatta UM, Ross IM, Sayle TXT, *et al.* Cationic surface reconstructions on cerium oxide nanocrystals: an aberration-corrected HRTEM study. ACS Nano, 2012, 6: 421–430
32 Möbus G, Saghi Z, Sayle DC, *et al.* Dynamics of polar surfaces on ceria nanoparticles observed *in situ* with single-atom resolution. Adv Funct Mater, 2011, 21: 1971–1976
33 Ling Y, Wang Z, Wang Z, *et al.* A robust carbon tolerant anode for solid oxide fuel cells. Sci China Mater, 2015, 58: 204–212
34 Capdevila-Cortada M, López N. Entropic contributions enhance polarity compensation for CeO_2 (100) surfaces. Nat Mater, 2016, 16: 328–334
35 Lin Y, Wu Z, Wen J, *et al.* Adhesion and atomic structures of gold on ceria nanostructures: the role of surface structure and oxidation state of ceria supports. Nano Lett, 2015, 15: 5375–5381

Acknowledgements This work was supported by the National natural Science Foundation of China (51525102, 51390475, 51371102 and 21673277) and the National Basic Research Program of China (2015CB654902). In this work we used the resources of the National Center for Electron Microscopy in Beijing and Shanghai Supercomputer Center.

Author contributions Yu R proposed and guided the project. Huang J performed image analysis and simulations. Yu Y synthesized the samples. Yu R performed TEM experiments and first-principles calculations. Huang J and Yu R wrote the manuscript. All authors discussed the results.

Conflict of interest The authors declare that they have no conflict of interest.

Jinglu Huang is a PhD candidate at the School of Materials Science and Engineering, Tsinghua University, under the supervision of Prof. Rong Yu. She received her Bachelor's degree from Zhejiang University in 2012. Her current research focuses on the atomic configuration and electronic structure of local structures in materials.

Rong Yu is a professor of the School of Materials Science and Engineering, Tsinghua University. He received bachelor's degree in 1996 from Zhejiang University, and PhD in 2002 from the Institute of Metal Research, Chinese Academy of Sciences. His research interests include surface science and catalysis of metals and oxides, microstructure of intermetallics, and structural transition and interfaces in transition metal oxides.

二氧化铈(100)表面的原子面反转

黄静露[1], 余运波[2,3,4], 朱静[1], 于荣[1*]

摘要 氧化铈表面的结构与性能对氧化铈材料的许多实际应用有着重要的影响, 因此受到了广泛的关注和研究. 由于大多数的表面技术仅限于获得表面最外层原子的结构信息, 对材料亚表面的结构信息还非常匮乏. 我们基于像差校正高分辨透射电子显微技术, 同时获得了氧化铈(100)表面和亚表面的结构信息, 从而揭示了氧化铈(100)表面的一种亚稳态. 在这种新结构中, 表面最外层和次外层原子面发生了反转, 使得具有Ce终结的化学计量比的表面以O原子面暴露在最外层. 伴随这种原子面反转, 为了补偿表面极性的电荷重排也不同于正常的(100)表面.